Systems & Control Transactions

Original Research Article
Peer Reviewed Conference Proceeding
ESCAPE 36 - European Symposium on Computer Aided Process Engineering
Sheffield, UK. 21-24 June 2026

PSE PRESS

A Framework based on Population Balance Modeling for Predicting Li–O_2 Battery Discharge and Life Cycle Behavior

Nadia G. Khouri[a*], Jean F. Leal Silva[a], Letícia M. S. Barros[a], Viktor O. C. Concha[b], Rubens Maciel Filho[a]

[a] University of Campinas (UNICAMP), School of Chemical Engineering, Campinas, São Paulo, Brazil
[b] Federal University of São Paulo (UNIFESP), School of Chemical Engineering, Diadema, São Paulo, Brazil
* Corresponding Author: nadiagk@unicamp.br.

ABSTRACT

The growing integration of renewable energy sources such as solar and wind power has intensified the demand for advanced energy storage technologies. Lithium–air (Li–O_2) batteries are particularly attractive due to their exceptionally high theoretical specific energy, which surpasses that of the conventional lithium-ion system. However, their practical application is hindered by poor reversibility during discharge, primarily due to the formation and decomposition of lithium peroxide (Li_2O_2), which causes cathode passivation and capacity fading. Since the electrochemical performance of Li–O_2 batteries is strongly influenced by the morphology, size, and spatial distribution of Li_2O_2 crystals, understanding the mechanisms governing their nucleation and growth is critical. To address this challenge, this work proposes a computational framework based on population balance modeling (PBM) to describe Li_2O_2 crystallization dynamics during battery discharge. The framework integrates population, mass, and energy balances, allowing the coupled analysis of electrochemical kinetics, supersaturation effects, and the evolution of crystal size distributions. Compared with continuum-scale and phase-field models, the PBM approach offers reduced computational cost while naturally accounting for particle size distributions and linking microscopic crystallization phenomena to macroscopic battery performance and degradation. Although simplified assumptions were adopted in this initial formulation, the framework successfully captures the essential discharge behavior of Li–O_2 systems. As such, it provides a robust foundation for future model refinements incorporating additional physicochemical mechanisms and more detailed electrochemical and transport phenomena.

Keywords: Batteries, Dynamic Modelling, Energy Storage, Energy Systems, Simulation, Population Balance

INTRODUCTION

Renewable energy sources represent a promising alternative to mitigate environmental issues associated with conventional fossil-based systems. In addition to their role in reducing greenhouse gas emissions, renewables have become increasingly cost-competitive in electricity generation. According to the International Renewable Energy Agency [1], solar photovoltaic (PV) and onshore wind technologies are significantly more economical than fossil fuel–based alternatives with costs approximately 41% and 53% lower than conventional options, respectively [2]. Despite their advantages, sources such as solar and wind are inherently intermittent. Solar power generation is constrained to daylight hours, while wind energy availability is dependent on geographic and meteorological conditions [3]. This intermittency is a challenge to the reliable and continuous supply of electricity that motivates the development of integrated energy systems capable of storing excess energy and delivering it on demand. In this context, electrochemical energy storage technologies, particularly batteries, have emerged as a viable solution to enable the large-scale integration of renewables. Notably, the cost of battery technologies has decreased more than 90% since 2010, highlighting their growing viability [2].

Rechargeable lithium-ion batteries have become the dominant energy storage technology for mobile app-

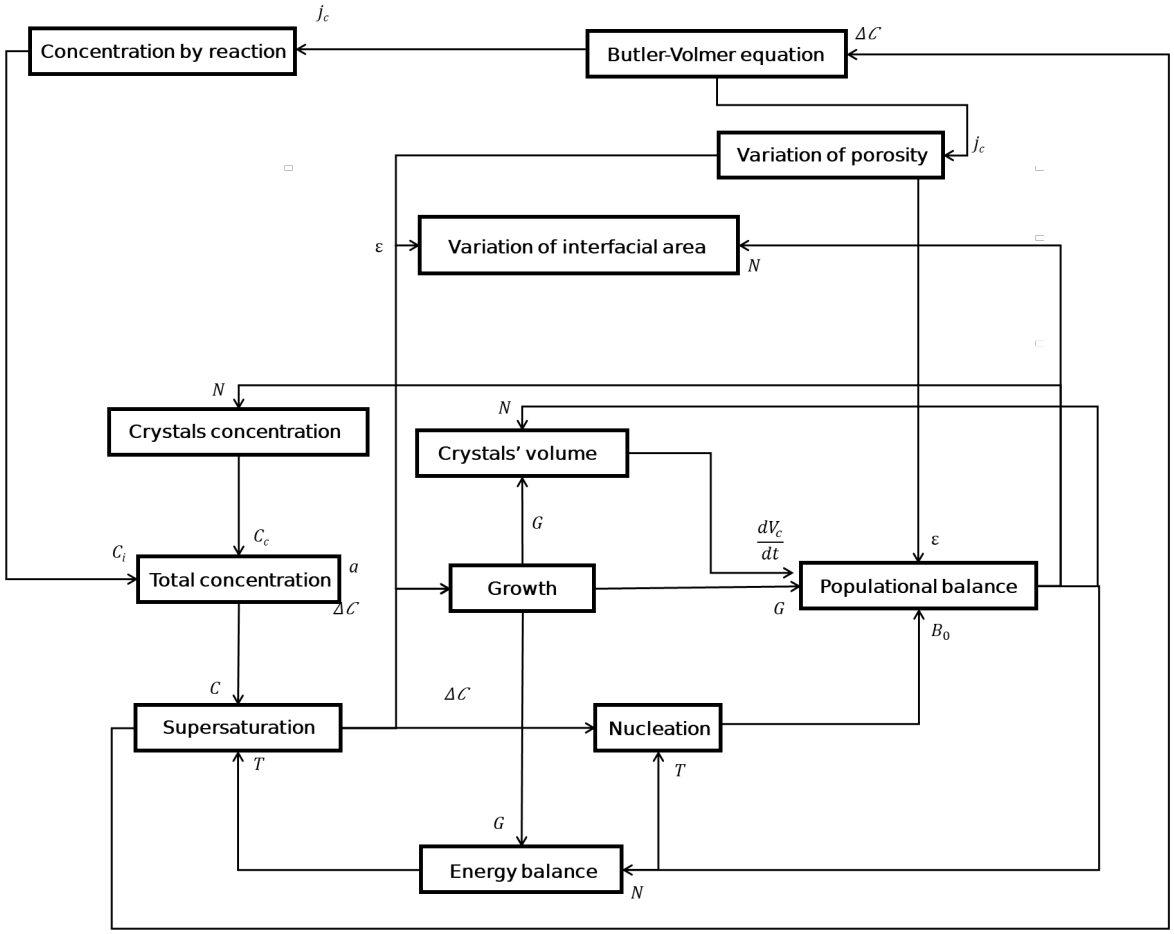

Figure 1. Information flow to model the discharge product involved in the Li_2-O_2 battery.

lications, largely due to their high energy density [4]. Despite these advantages, the energy density of lithium-ion batteries is approaching its theoretical limit and remains insufficient to fully meet the growing global demand for large-scale storage. In this context, lithium–air (Li–O_2) batteries have attracted attention because of their high theoretical specific energy, reported to reach approximately 3500 W.h/kg [5]. Nevertheless, this value is unlikely to be achieved in practical systems due to fundamental challenges [6].

In lithium–oxygen (Li–O_2) batteries, the overall reversible electrochemical reaction is governed by the formation and decomposition of lithium peroxide (Li_2O_2), in contrast to the intercalation-based mechanism of conventional lithium-ion batteries [7]. The morphology and accumulation of the Li_2O_2 discharge product are critical factors influencing the performance and reversibility of Li–O_2 cells. Specifically, Li_2O_2 formation and decomposition at the cathode directly affect round-trip efficiency, rate capability, and long-term cycling stability [8]. Studies have demonstrated that the insulating Li_2O_2 can deposit in diverse morphologies, including thin films and complex toroidal structures, depending on operating conditions [9]. Since the crystallization form of Li_2O_2 governs electron transport pathways and reaction accessibility during charging, controlling its morphology is essential. Consequently, a detailed understanding of how process variables influence Li_2O_2 nucleation, growth, and morphology is essential for optimizing battery capacity and achieving stable, reversible Li–O_2 operation.

Motivated by the influence of Li_2O_2 crystallization in the performance of Li–O_2 batteries, previous theoretical studies based on experimental observations have examined the formation of discharge products during battery operation [10-12]. In earlier work by the authors, a population balance–based model was applied to analyze Li_2O_2 deposition during discharge, and the resulting trends and performance-related implications were discussed [13]. The present study, however, addresses a distinct and complementary objective. Rather than focusing on the interpretation of modeling outcomes, this work provides a detailed exposition of the population balance modeling framework itself, including the governing equations, assumptions, numerical implementation, and coupling with

electrochemical variables. By systematically elucidating the structure and rationale of the model, this contribution establishes a reproducible simulation platform for Li_2O_2 crystallization, with direct applicability to other battery systems in which crystallization processes are crucial. As such, the novelty of this work lies in the formalization and clarification of the modeling methodology, enabling its reliable application and future expansion to more complex electrochemical energy storage systems.

LI-O2 CRYSTALLIZATION MODELLING

Crystallization produces solid particles with a distribution of sizes, commonly described by the crystal size distribution (CSD). In Li–O_2 batteries, the evolution of the CSD during discharge is governed by the coupled effects of electrochemical kinetics, mass and energy transport, and particle population dynamics. These phenomena are captured through an integrated modeling framework that accounts for Li_2O_2 saturation, nucleation, and crystal growth (Figure 1). Accordingly, the following sections detail the core components of the model, including the characterization of Li_2O_2 crystals, mass and energy balances coupled with electrochemical kinetics, the population balance formulation, and the expressions adopted for saturation, nucleation, and growth rates.

Characteristics of Li2O2 crystals

The external geometry of a crystal can be characterized by its characteristic length (L), the surface areas of its facets, and the angles between them. In modeling applications, these geometric attributes are conveniently represented through shape factors, which provide a compact description of crystal morphology. Shape factors are commonly defined with respect to crystal volume and surface area, as expressed by the volume-based and area-based shape factors (Equations 1 and 2), respectively [14]. These dimensionless parameters relate the characteristic length of a crystal to its corresponding volume and surface area. In the case of lithium peroxide, experimental observations indicate that the discharge product typically forms disk-like structures, such as toroids or oblate spheroids. Consequently, the associated shape factors are functions of the aspect ratio between the disk diameter and thickness, which governs the effective morphology of Li_2O_2 crystals [15].

$$V_c = k_V L^3 \tag{1}$$

$$A_c = k_a L^2 \tag{2}$$

Mass balance of Li_2O_2 crystals and kinetics

The material balance of Li_2O_2 crystals during battery discharge is formulated by accounting for the temporal accumulation of solid discharge products within the cathode. Equation 3 quantifies the total mass of Li_2O_2 as obtained from the distribution of insoluble crystals in the system and Equation 4 describes the evolution of crystal volume as a function of particle growth. To close the mass balance, the rate of Li_2O_2 formation must be linked to the underlying electrochemical processes. Lithium peroxide is generated through the cathodic oxygen reduction reaction, and its formation rate is evaluated using the Butler–Volmer formulation (Equation 5). This expression captures the dependence of the reaction rate on the applied overpotential as well as on the concentrations of the reactants (O_2 and Li^+) and the discharge product (Li_2O_2). Based on the calculated cathodic reaction rate, the resulting variations in Li_2O_2 concentration, electrode porosity, and electrochemically active interfacial area are subsequently determined (Equations 6–8). Finally, the effective suspension volume of the system (Vsusp) is estimated from the geometric dimensions of the cathode (radius and thickness) in combination with the evolving porosity (Equation 9) [16].

$$C_c(t) = k_V \rho_c \int_0^\infty N(L,t) L^3 dL \tag{3}$$

$$\frac{dV_c}{dt} = -3k_V \int_0^\infty G(L,t) N(L,t) L^2 dL \tag{4}$$

$$\frac{j_c}{nF} = k_{ano} \Delta C exp\left[\frac{(1-\beta)nF}{RT}\eta_c\right] - k_c (C_{Li})^2 C_{O_2} exp\left[\frac{-\beta nF}{RT}\eta_c\right] \tag{5}$$

$$\frac{\partial C_i}{\partial t} = -\frac{a j_c MM}{2F} \tag{6}$$

$$\frac{\partial \varepsilon}{\partial t} = \frac{a j_c MM}{2F\rho_c} \tag{7}$$

$$ae = ae_0 \left[1 - \left(\frac{k_v \int_0^\infty N L^3 dL}{V_{susp}\varepsilon_0}\right)\right]^p \tag{8}$$

$$V_{susp} = \pi r_{el}{}^2 esp\, \varepsilon \tag{9}$$

Energy balance

The energy balance describes the heat transfer processes occurring within the system and is expressed by Equation 10. Two primary contributions are considered in this formulation. The first accounts for the thermal effects associated with crystallization and Li_2O_2 formation, represented by the crystallization enthalpy. The second term represents heat exchange with the surroundings. In the present model, heat dissipation to the environment is assumed to occur via forced air convection, characterized by an average overall heat transfer coefficient of 30 W m^{-2} K^{-1} [17].

$$\rho_e c_{p_e} \frac{dT}{dt} = \left(-3\Delta H_c \rho_c k_V \int_0^\infty G(L,t)N(L,t)L^2 dL\right) - UA_T(T - T_s) \quad (10)$$

Populational Balance

The general population balance equation (PBE) employed in this work was previously derived and reported by the authors in an earlier study (Equation 11) [18].

$$\frac{\partial N_\xi}{\partial t} + \frac{\partial}{\partial x} \bullet (U_o N_\xi) + \frac{\partial}{\partial \xi} \bullet (\dot{\xi} N_\xi) = h_\xi \quad (11)$$

Building on this formulation, several assumptions were adopted to tailor the population balance description to Li–O_2 battery systems. Crystal size is characterized using a single linear dimension, namely the characteristic length L, resulting in a univariate population balance (ξ=L). The system is modeled under transient operating conditions, reflecting the time-dependent nature of battery discharge. The control volume is defined as the cathode surface, which constitutes the primary site of Li_2O_2 nucleation and growth. Accordingly, the corresponding term in the PBE accounts for temporal changes in particle volume within the electrode domain. Particle transport within the phase volume is assumed to be governed solely by the linear crystal growth rate, while birth and death processes associated with discrete events are neglected (h_ξ =0). Under these assumptions, the population balance for Li_2O_2 crystallization reduces to the batch crystallizer formulation expressed in Equation 12, yielding a partial differential equation that depends on both particle size and time, N(L, t). Two boundary conditions are required to close the system: the first, N(0, t), represents the nucleation flux (Equation 13), while the second, N(L, 0), corresponds to the initial seed crystal size distribution. The resulting PBE is solved numerically using the method of classes, in which the size domain is discretized into finite intervals, transforming the PDE into a system of ordinary differential equations with established numerical solution procedures (Equations 14–16).

$$\frac{\partial N}{\partial t} + \frac{\partial (GN)}{\partial L} + N\frac{\partial V}{V \partial t} = 0 \quad (12)$$

$$N(0,t) = \frac{B_0(t)}{G(0,t)} \quad (13)$$

$$\frac{dN_1}{dt} + \frac{1}{V_{susp}}\frac{dV_c}{dt}N_1 + \frac{G(L_1)}{2\Delta c_1}N_1 + \frac{G(L_1)}{2\Delta c_2}N_2 = B_0 \quad (14)$$

$$\frac{dN_i}{dt} + \frac{1}{V_{susp}}\frac{dV_c}{dt}N_i + \frac{G(L_i)}{2\Delta c_{i+1}}N_{i+1} + \frac{G(L_i) - G(L_{i-1})}{2\Delta c_i}N_i - \frac{G(L_{i-1})}{2\Delta c_{i-1}}N_{i-1} = 0 \quad (15)$$

$$\frac{dN_N}{dt} + \frac{1}{V_{susp}}\frac{dV_c}{dt}N_N - \frac{G(L_{N-1})}{2\Delta c_N}N_N - \frac{G(L_{N-1})}{2\Delta c_{N-1}}N_{N-1} = 0 \quad (16)$$

Crystal saturation

A solution is defined as saturated when thermodynamic equilibrium is established between a dissolved species and its corresponding solid phase, indicating that the maximum solute concentration permitted under given conditions has been reached. Saturation is therefore an intrinsic property of the solute–solvent system and is strongly dependent on temperature [19]. In most cases, solubility increases with temperature; however, certain systems exhibit weak temperature dependence or even a decrease in solubility as temperature rises. In contrast, supersaturation arises when the solute concentration in the solution exceeds its equilibrium saturation value. The degree of supersaturation (ΔC) is quantified as the difference between the actual solute concentration (C) and the equilibrium saturation concentration (C∗), as defined in Equation 17. Supersaturated systems are thermodynamically unstable and provide the driving force for nucleation and crystal growth, making supersaturation important in crystallization processes.

$$\Delta C = C - C^* \quad (17)$$

Nucleation rate (B0)

Nucleation refers to the formation of stable crystal embryos from a supersaturated solution, marking the onset of a new solid phase. In this work, the nucleation rate of Li_2O_2 is modeled using classical nucleation theory [20]. For disk-shaped nuclei, the free energy of formation is evaluated by considering a critical nucleus size that ensures thermodynamic stability and sustained growth (Equation 18) [9]. The corresponding surface energy (γ) is estimated using the correlation given in Equation 19 [19]. On this basis, the nucleation rate expression (Equation 20) is formulated as a function of the Zeldovich factor (Equation 21), the diffusion coefficient of Li_2O_2 in the electrolyte (Equation 25), and the density of active nucleation sites (x0) The parameter x0 must be estimated for the system and represents one of the principal sources of uncertainty in the model. Accordingly, its influence on the predicted crystallization behavior is examined in detail in the previous work [13].

$$G_{crit} = \frac{\gamma^2 a^4}{2k_b T \ln(dC/C^*)} \quad (18)$$

$$\gamma = 0.414\, k_b T \ln(dC/C^*)\left(\frac{dC * Na}{MM_{Li_2O_2}}\right)^{2/3} \quad (19)$$

$$B_0 = D_l a_D^{-2} Z x_0 \exp\left(\frac{-G_{crit}}{k_b T}\right) \quad (20)$$

$$Z = \frac{[G_{crit}/(3\pi k_b T)]^{0.5}}{n_{crit}} \quad (21)$$

Growth rate (G)

The crystal growth rate, G, is defined as the temporal rate of change of the characteristic crystal length, dL/dt and is evaluated using the expression given in Equation 22. To account for the interplay between electrochemical reaction kinetics and mass transport limitations, an effectiveness factor for Li_2O_2 growth, ηr, is introduced and calculated according to Equation 23. This factor quantifies the relative contributions of reaction-controlled and diffusion-controlled growth regimes. Low values of effectiveness indicate dominance of the electrochemical reaction rate constant (k_c), whereas values approaching unity signify growth primarily limited by mass transfer, characterized by the mass transfer coefficient (kd). The coefficient kd is determined using Equation 24, as described in the literature [21-22]. The parameter θ represents the ratio of the operating current density to the limiting current density, with the latter corresponding to conditions under which reactant depletion in the electrolyte or membrane induces concentration polarization and constrains mass transport [23]. Finally, the diffusivity of disk-shaped Li_2O_2 crystals, D_l, is calculated using Equation 25 [24], which is derived from the linear regime observed in the early-time response of the curve obtained from intermittent potentiostatic titration experiments. The constant ksl corresponds to the slope of this linear relationship.

$$G = \frac{k_a k_c MM}{3\rho_c k_V}\eta_r(\Delta C)^{j_l} \quad (22)$$

$$\eta_r = \frac{1}{\frac{k_c}{k_d}(\Delta C) + 1} \quad (23)$$

$$k_d = \frac{I_c K_R RT}{8F^3(C_{Li_2O_2}/MM)^2 D_l\, \theta\, ae\, esp} \quad (24)$$

$$D_l = \left(\frac{\pi}{36}\right)\left(\frac{k_{sl}\, L}{Q}\right)^2 \quad (25)$$

COMPUTATIONAL IMPLEMENTATION

The computational implementation of the proposed modeling framework follows the information flow illustrated in Figure 1, integrating all key components required to describe crystallization phenomena in battery systems. The system of ordinary differential equations resulting from the discretized population balance formulation was solved using the *solve_ivp* routine from the SciPy library, employing the implicit multistep Backward Differentiation Formula (BDF) method. This solver was selected for its robustness and numerical stability when handling stiff systems arising from the strong coupling between crystallization kinetics and electrochemical processes.

The discretization of the particle size domain required by the method of classes is inherently system-dependent and must be defined according to the characteristic crystal sizes, growth kinetics, and operating conditions of the electrochemical system under investigation. Both the extent of the size domain and the class width should therefore be chosen to adequately resolve the evolution of the crystal size distribution. In the present implementation, and consistent with the methodology established in the authors' previous work, the size domain was discretized using a uniformly spaced mesh spanning from 0 to 10 μm, with a class width of 0.05 μm. This discretization was shown to be appropriate for capturing the order of magnitude and temporal evolution of Li_2O_2 crystal growth during battery discharge. A uniform mesh was adopted because the population dynamics are governed exclusively by continuous nucleation and growth processes, with no contribution from discrete birth or death events.

The integral terms appearing in the mass and energy balance equations were evaluated using the *integrate.quad* function from the SciPy library, ensuring accurate numerical integration over the discretized size domain. Following implementation, the model outputs were systematically compared against selected response variables to verify numerical consistency and proper coupling among the governing equations, thereby validating the computational methodology employed in this study.

CONCLUSION

In this work, a population balance–based modeling framework was developed to describe the crystallization occurring during the discharge of Li–O_2 batteries. To enable an adequate formulation, several simplifying assumptions were adopted, which limit the quantitative accuracy of the model and its ability to capture highly complex operating scenarios, such as variable discharge currents, electrolyte compositions, or detailed electrode architectures. A key strength of the proposed approach lies in its ability to naturally account for crystal size distributions and morphological effects while maintaining a relatively low computational cost. By bridging microscopic crystallization mechanisms with macroscopic battery performance indicators, the framework provides physically meaningful insights without requiring excessively complex formulations. As such, it offers an accessible and flexible modeling platform for investigating crystallization-driven limitations in metal–air batteries. This study represents a step toward the systematic application of population balance modeling to Li–O_2 batteries, with a particular emphasis on formalizing and clarifying the

governing equations and numerical implementation. Future work may extend the present framework by incorporating additional mechanisms, such as side reactions, electrolyte-dependent effects, dynamic operating conditions, and alternative electrode designs. These developments would further enhance the predictive capability.

Symbology

a_e = interfacial area.
a_D = length scale of liquid Li_2O_2.
A_C = surface area of the crystals.
A_T = thermal exchange area.
B_0 (t)= nucleation function.
c_p = specific heat.
C = concentration.
C* = equilibrium saturation concentration
ΔC = supersaturation.
D_l= diffusivity constant of crystals.
esp = electrode thickness.
F = Faraday constant.
G^{crit} = critical formation energy of crystal nuclei.
G(L, t) = crystal growth function.
h_ξ = jump function (discrete events).
H_c = heat of formation.
I_c = current applied to the system.
j_c = interfacial transfer current density.
j_l = kinetic order of the growth law.
k_a = constant to obtain the crystal surface area.
k_{ano} = anodic kinetic constant.
k_b = Boltzmann constant.
k_c = cathodic kinetic constant.
k_d= mass transfer coefficient.
k_{sl}= diffusivity constant of the Li2O2 crystal.
k_v= constant to obtain the volume of the crystal.
K_r = electrolyte conductivity.
L = characteristic length.
MM = molar mass.
n = number of electrons in the reaction.
n_{crit} = critical nucleus size.
N = total number density.
N_A = Avogadro's number.
Q = battery capacity.
rel= electrode radius.
R = universal gas constant.
t = discharge time.
T = temperature.
U = overall heat transfer coefficient.
U_o = crystals velocity.
x_0 = nucleation site density.
V_c= volume of the crystals.
V_{susp}= effective volume of the system.
Z = Zeldovish factor.
ξ = internal coordinate vector of the PB.
ε = electrode porosity.
ρ_c = specific mass of Li2O2 crystals.
ρ_e= specific mass of the electrolyte.
η_r= effectiveness factor.
η_c= overpotential.
γ= surface energy.
θ = ratio of current density to limiting current density.

ACKNOWLEDGEMENTS

The authors acknowledge the financial support provided by the National Council for Scientific and Technological Development (CNPq, Brazil), the Coordenação de Aperfeiçoamento de Pessoal de Nível Superior (CAPES, Brazil; Finance Code 001), and the São Paulo Research Foundation (FAPESP, Brazil) through Grant Nos. 2018/16663-2, 2023/08594-9, and the Thematic Project Grant No. 2022/16379-8. The authors also gratefully acknowledge the Universidade Estadual de Campinas (UNICAMP) and the School of Chemical Engineering, Campinas, SP, Brazil, for the institutional support provided during the development of this work.

AUTHOR IDENTIFIERS

Author ORCIDs:
Khouri NG: 0000-0002-2954-4947
Leal Silva JF: 0000-0002-9915-5859
Barros LMS: 0000-0002-9786-8783
Concha VOC: 0000-0002-3520-4535
Maciel Filho R: 0000-0001-6511-7283

REFERENCES

1. International Renewable Energy Agency. *Renewable energy statistics 2025* https://www.irena.org/-/media/Files/IRENA/Agency/Publication/2025/Jul/IRENA_DAT_RE_Statistics_2025.pdf
2. Reuters.https://www.reuters.com/business/energy/around-90-renewables-cheaper-than-fossil-fuels-worldwide-irena-says-2025-07-22
3. Conde HJC, Demition CM, Honra J. Storage is the new black: a review of energy storage system applications to resolve intermittency in renewable energy systems. Energies 18:354 (2025). https://doi.org/10.3390/en18020354
4. Adelhelm P, Hartmann P, Bender CL, Busche M, Eufinger C, Janek J. From lithium to sodium: cell chemistry of room temperature sodium–air and sodium–sulfur batteries. Beilstein J. Nanotechnol. 6:1016-1055 (2015). https://doi.org/10.3762/bjnano.6.105
5. Lampic G, Gotovac G, Geaney H, O'Dwyer C. Comparing the suitability of lithium ion, lithium sulfur and lithium air batteries for current and future vehicular applications. arXiv preprint

2016.06347 (2016) https://doi.org/10.48550/arXiv.1606.06347
6. Deng F, Zhang Y, Yu Y. Conductive metal–organic frameworks for rechargeable lithium batteries. Batteries 9:109 (2023). https://doi.org/10.3390/batteries9020109
7. Li S, Liu Y, Wu X, Wang K, Chen J. Tailoring the growth and morphology of lithium peroxide: nickel sulfide/nickel phosphate nanotubes with optimized electronic structure for lithium–oxygen batteries. Small 19: (2023). https://doi.org/10.1002/smll.202304435
8. Huang X, Li M, Gao Y, Park MG, Matsuda S, Amine K. Discharge rate?driven li ₂ o ₂ growth exhibits unconventional morphology trends in solid?state li?o ₂ batteries. Angew Chem Int Ed 64: (2025). https://doi.org/10.1002/anie.202507967
9. Horstmann B, Gallant B, Mitchell R, Bessler WG, Shao-Horn Y, Bazant MZ. Rate-dependent morphology of li₂o₂ growth in li–o₂ batteries. J. Phys. Chem. Lett. 4:4217-4222 (2013). https://doi.org/10.1021/jz401973c
10. Wang Y. Modeling discharge deposit formation and its effect on lithium-air battery performance. Electrochimica Acta 75:239-246 (2012). https://doi.org/10.1016/j.electacta.2012.04.137
11. Lau S, Archer LA. Nucleation and growth of lithium peroxide in the li–o₂ battery. Nano Lett. 15:5995-6002 (2015). https://doi.org/10.1021/acs.nanolett.5b02149
12. Yin Y, Gaya C, Torayev A, Thangavel V, Franco AA. Impact of li₂o₂ particle size on li–o₂ battery charge process: insights from a multiscale modeling perspective. J. Phys. Chem. Lett. 7:3897-3902 (2016). https://doi.org/10.1021/acs.jpclett.6b01823
13. Gagliardi Khouri N, Leal Silva JF, Sampaio Barros LM, Cárdenas Concha VO, Maciel Filho R. Lithium peroxide crystallization in lithium-air batteries: a population balance modeling approach to enhance energy storage. Journal of Energy Storage 140:118939 (2025). https://doi.org/10.1016/j.est.2025.118939
14. Costa CBB. Modelagem e controle ótimo do processo de cristalização do ácido adípico. PhD Thesis, Universidade Estadual de Campinas (2003) http://repositorio.unicamp.br/bitstream/REPOSIP/266500/1/Costa_CalianeBastosBorba_M.pdf
15. Endo Y, Chen R, Pui DYH. Theoretical consideration of permeation resistance of fluid through a particle packed layer. Powder Technology 124:119-126 (2002). https://doi.org/10.1016/s0032-5910(01)00479-x
16. Jiang K, Liu X, Lou G, Wen Z, Liu L. Parameter sensitivity analysis and cathode structure optimization of a non-aqueous li–o2 battery model. Journal of Power Sources 451:227821 (2020). https://doi.org/10.1016/j.jpowsour.2020.227821
17. Ling Z, Wang F, Fang X, Gao X, Zhang Z. A hybrid thermal management system for lithium ion batteries combining phase change materials with forced-air cooling. Applied Energy 148:403-409 (2015). https://doi.org/10.1016/j.apenergy.2015.03.080
18. Khouri NG, Bahú JO, Miranda NT, Batistella CB, Maciel MRW, Concha VOC, Maciel Filho R. Diesel upgrading: a modeling of its microemulsions. Fuel Processing Technology 239:107545 (2023). https://doi.org/10.1016/j.fuproc.2022.107545
19. Mersmann A. Calculation of interfacial tensions. Journal of Crystal Growth 102:841-847 (1990). https://doi.org/10.1016/0022-0248(90)90850-k
20. Kashchiev D, van Rosmalen GM. Review: nucleation in solutions revisited. Cryst. Res. Technol. 38:555-574 (2003). https://doi.org/10.1002/crat.200310070
21. Yuan H, Read JA, Wang Y. Capacity loss of non-aqueous li-air battery due to insoluble product formation: approximate solution and experimental validation. Materials Today Energy 14:100360 (2019). https://doi.org/10.1016/j.mtener.2019.100360
22. Barton JL, Milshtein JD, Hinricher JJ, Brushett FR. Quantifying the impact of viscosity on mass-transfer coefficients in redox flow batteries. Journal of Power Sources 399:133-143 (2018). https://doi.org/10.1016/j.jpowsour.2018.07.046
23. La Cerva M, Gurreri L, Tedesco M, Cipollina A, Ciofalo M, Tamburini A, Micale G. Determination of limiting current density and current efficiency in electrodialysis units. Desalination 445:138-148 (2018). https://doi.org/10.1016/j.desal.2018.07.028
24. Gallant BM, Kwabi DG, Mitchell RR, Zhou J, Thompson CV, Shao-Horn Y. Influence of li2o2 morphology on oxygen reduction and evolution kinetics in li–o2 batteries. Energy Environ. Sci. 6:2518 (2013). https://doi.org/10.1039/c3ee40998h

© 2026 by the authors. Licensed to PSEcommunity.org and PSE Press. This is an open access article under the creative commons CC-BY-SA licensing terms. Credit must be given to creator and adaptations must be shared under the same terms. See https://creativecommons.org/licenses/by-sa/4.0/